ERJ open research
THE BEST IN OPEN ACCESS BASIC, TRANSLATIONAL & CLINICAL RESPIRATORY RESEARCH

Early View

Original Research Article

Exploring glucocorticoid receptor signaling in lymphangioleiomyomatosis

Alexandra Baiges, Lara Ruiz-Auladell, Irene García, Raúl Rigo-Bonnin, Yan Tang, Elias J. Bou-Farhat, Roderic Espín, Rosario T. Sanz, Guillermo Pablo Vicent, Mercè Donate, Arzoo Shabbir, Jonathan Adams, Carmen Herranz-Ors, Rosalía Laporta, Clara Salas, Piedad Ussetti, Claudia Valenzuela, Julio Ancochea, José A. Rodríguez-Portal, María Molina-Molina, Álvaro Casanova, Eva Revilla-López, Luis Gómez-Carrera, Xavier Matias-Guiu, Miguel Angel Pavón, Dominik Jung, Hagen S. Bachmann, Ramón Manuel Lago-Lestón, Laura Muinelo-Romay, Xavier Farré, Rafael de Cid, Calvin S. Leung, Anthony S. Zannas, Manel Esteller, Jacobo Sellares, Katarzyna Błasińska, Adriana Róży, Paulina Skrońska, Antonio Gómez, Marina K. Holz, Julie S. Di Martino, David Monk, Charlotte Sefton, Leanne Walker, Anne White, Debbie Clements, Suzanne Miller, Simon R. Johnson, Hazel J. Hunt, Elizabeth P. Henske, David Kwiatkowski, Elżbieta Radzikowska, Francesca Mateo, Miquel Angel Pujana

Please cite this article as: Baiges A, Ruiz-Auladell L, García I, *et al*. Exploring glucocorticoid receptor signaling in lymphangioleiomyomatosis. *ERJ Open Res* 2026; in press (https://doi.org/10.1183/23120541.01285-2025).

Exploring glucocorticoid receptor signaling in lymphangioleiomyomatosis

Alexandra Baiges[1]†, Lara Ruiz-Auladell[1]†, Irene García[1]†, Raúl Rigo-Bonnin[2], Yan Tang[3], Elias J Bou-Farhat[3], Roderic Espín[1], Rosario T Sanz[4], Guillermo Pablo Vicent[4], Mercè Donate[5], Arzoo Shabbir[1], Jonathan Adams[1], Carmen Herranz-Ors[1]‡, Rosalía Laporta[6], Clara Salas[7], Piedad Ussetti[6], Claudia Valenzuela[8], Julio Ancochea[8], José A Rodríguez-Portal[9,10], María Molina-Molina[10,11], Álvaro Casanova[12], Eva Revilla-López[13], Luis Gómez-Carrera[10,14,15], Xavier Matias-Guiu[16,17], Miguel Angel Pavón[18,19], Dominik Jung[20], Hagen S Bachmann[20], Ramón Manuel Lago-Lestón[21], Laura Muinelo-Romay[17,21,22], Xavier Farré[23,24], Rafael de Cid[23,24], Calvin S Leung[25,26], Anthony S Zannas[26-29], Manel Esteller[17,30-32], Jacobo Sellares[33], Katarzyna Błasińska[34], Adriana Róży[34], Paulina Skrońska[34], Antonio Gómez[35], Marina K Holz[36], Julie S Di Martino[36], David Monk[37], Charlotte Sefton[38], Leanne Walker[38], Anne White[38], Debbie Clements[39], Suzanne Miller[39,40], Simon R Johnson[39,40], Hazel J Hunt[41], Elizabeth P Henske[3], David Kwiatkowski[3], Elżbieta Radzikowska[34], Francesca Mateo[1], and Miquel Angel Pujana[1,5]*

1 ProCURE, Catalan Institute of Oncology, Bellvitge Institute for Biomedical Research (IDIBELL), L'Hospitalet del Llobregat, Barcelona, Spain
2 Department of Biochemistry and Molecular Genetics, Biomedical Diagnostic Center (CDB), Hospital Clinic de Barcelona, Barcelona, Spain
3 Division of Pulmonary and Critical Care Medicine, Brigham and Women's Hospital, Harvard Medical School, Boston, Massachusetts, United States of America
4 Molecular Biology Institute of Barcelona, Spanish National Research Council (IBMB-CSIC), Barcelona, Spain
5 Precision Oncology in Girona (OncoGir), Girona Institute for Biomedical Research (IDIBGI), Salt, Girona, Spain
6 Pneumology Service, University Hospital Clínica Puerta del Hierro, Majadahonda, Madrid, Spain
7 Department of Pathology, University Hospital Clínica Puerta del Hierro, Majadahonda, Madrid, Spain
8 Pneumology Service, La Princesa Research Institute, University Hospital La Princesa, Madrid, Spain
9 Medical-Surgical Unit of Respiratory Diseases, University Hospital Virgen del Rocío, Institute of Biomedicine of Seville (IBiS), Seville, Spain
10 Network Center for Biomedical Research on Respiratory Diseases (CIBERES), Institute of Health Carlos III, Madrid, Spain
11 Interstitial Lung Disease Unit, Department of Respiratory Medicine, University Hospital of Bellvitge, IDIBELL, L'Hospitalet del Llobregat, Barcelona, Spain
12 Pneumology Service, University Hospital of Henares, University Francisco de Vitoria, Coslada, Madrid, Spain
13 Pneumology Service, Vall d'Hebron University Hospital, Barcelona, Spain
14 Department of Respiratory Medicine, University Hospital La Paz, Research Institute University Hospital La Paz (IdiPAZ), Madrid, Spain
15 Department of Medicine, Autonomous University of Madrid, Madrid, Spain
16 Arnau de Vilanova University Hospital, Institute for Biomedical Research of Lleida (IRBLleida), University of Lleida, Lleida, Spain
17 Network Center for Biomedical Research on Cancer (CIBERONC), Institute of Health Carlos III, Madrid, Spain
18 Cancer Epidemiology Research Program, Catalan Institute of Oncology, IDIBELL, L'Hospitalet del Llobregat, Barcelona, Spain
19 Network Center for Biomedical Research on Epidemiology and Public Health Cancer (CIBERESP), Institute of Health Carlos III, Madrid, Spain
20 Institute of Pharmacology and Toxicology, Centre for Biomedical Education and Research (ZBAF), School of Medicine, Faculty of Health, Witten/Herdecke University, Witten, Germany
21 Liquid Biopsy Analysis Unit, Translational Medical Oncology (Oncomet), Health Research Institute of Santiago (IDIS), Santiago de Compostela, Spain
22 Galician Precision Oncology Research Group (ONCOGAL), Medicine and Dentistry School, University of de Santiago de Compostela (USC), Santiago de Compostela, Spain

23 Genomes for Life - GCAT Lab Group, CORE Program, Institute Germans Trias i Pujol (IGTP), Badalona, Spain
24 Research Group on the Impact of Chronic Diseases and Their Trajectories (GRIMTra), IGTP, Badalona, Spain
25 Department of Molecular Biology, Cell Biology and Biochemistry, Brown University, Providence, Rhode Island, United States of America
26 Department of Psychiatry, University of North Carolina at Chapel Hill, Chapel Hill, North Carolina, United States of America
27 Department of Genetics, University of North Carolina at Chapel Hill, Chapel Hill, North Carolina, United States of America
28 Carolina Stress Initiative, University of North Carolina at Chapel Hill, Chapel Hill, North Carolina, United States of America
29 Institute for Trauma Recovery, University of North Carolina at Chapel Hill, Chapel Hill, North Carolina, United States of America
30 Cancer Epigenetics Group, Josep Carreras Leukemia Research Institute (IJC), Badalona, Barcelona, Spain
31 Catalan Institution for Research and Advanced Studies (ICREA), Barcelona, Catalonia, Spain
32 Physiological Sciences Department, School of Medicine and Health Sciences, University of Barcelona (UB), Barcelona, Spain
33 Pneumology Department, Hospital Clinic de Barcelona, August Pi i Sunyer Biomedical Research Institute (IDIBAPS), Barcelona, Spain
34 Department of Lung Diseases III, National Tuberculosis and Lung Diseases Research Institute, Warsaw, Poland
35 Biosciences Department, Faculty of Sciences and Technology (FCT), University of Vic – Central University of Catalonia (UVic-UCC), Vic, Spain
36 Departments of Cell Biology and Anatomy, New York Medical College, Valhalla, New York, United States of America
37 School of Biological Sciences, University of East Anglia, Norwich, United Kingdom
38 Division of Diabetes, Endocrinology, and Gastroenterology, School of Medical Sciences, Faculty of Biology, Medicine and Health, University of Manchester, Manchester, United Kingdom
39 Centre for Respiratory Research, Translational Medical Sciences, Biodiscovery Institute, National Institute for Health and Care Research (NIHR), Nottingham Biomedical Research Centre, University of Nottingham, UK
40 National Centre for Lymphangioleiomyomatosis, Nottingham University Hospitals NHS Trust, Nottingham, United Kingdom
41 Corcept Therapeutics, Redwood City, California, United States of America

†These authors contributed equally to this work
‡Present address: Wellcome Sanger Institute, Cambridge, United Kingdom
*Corresponding author: mapujana@iconcologia.net

Abstract

Background. Lymphangioleiomyomatosis (LAM) is a rare, low-grade neoplasm that causes progressive cystic lung destruction and is often associated with renal angiomyolipomas (AMLs). Given evidence of pleiotropy linking LAM risk to pulmonary traits, we investigated whether glucocorticoid receptor (GR) signaling might influence LAM biology and clinical features.

Methods. We combined cell-based studies, GR inhibition/activation assays, gene expression and single-cell RNA sequencing analyses, and hormone profiling in retrospective and prospective LAM cohorts. Cellular experiments employed murine *Tsc2*–/– embryonic fibroblasts and human *TSC2*–/– AML cells. Circulating steroid levels were measured in women with LAM and healthy controls, and associations with clinical variables were evaluated.

Results. In LAM/AML models, GR activation by glucocorticoids elicited transcriptional responses, whereas GR inhibition reduced clonogenic potential. GR stimulation was associated with *CDKN1C* upregulation through enhancer binding, and single-cell profiling suggested a shift toward slower proliferation and differentiation-prone states enriched for a LAM cell signature. Clinically, our analyses suggest that women with LAM may show altered circulating hormone profiles, including elevated ACTH and cortisol levels, together with reduced 17-hydroxyprogesterone, compared with controls. In a prospective cohort, ACTH levels were suggestively associated with advanced radiologic disease stage. AML cells showed elevated expression of *POMC*, which encodes the precursor of ACTH, and POMC peptide was detected in LAM lung tissue.

Conclusions. Our findings suggest that GR signaling may contribute to aspects of LAM cell behavior and disease status. Further investigation of this pathway could clarify its role as a disease modifier and potential therapeutic target.

Introduction

Lymphangioleiomyomatosis (LAM) is a rare, low-grade metastatic neoplasm that primarily affects women and is characterized by progressive cystic destruction of the lungs (1). Extrapulmonary involvement is common and typically includes renal angiomyolipomas (AMLs) and lymphatic abnormalities (2). Most clinical cases are sporadic (S-LAM), arising from somatic inactivation of the tumor suppressor gene *TSC2*, or less commonly *TSC1* (3). However, the precise cell of origin remains unknown (1). LAM also occurs in the context of Tuberous Sclerosis Complex (TSC), a multisystem disorder caused by germline or mosaic mutations in the same genes. In both S-LAM and TSC-LAM, loss of *TSC* gene product function leads to hyperactivation of the mechanistic target of rapamycin complex 1 (mTORC1), a key regulator of cell growth and metabolism (4). Estrogen signaling further promotes LAM cell survival and dissemination (5), yet disease onset and progression are typically slow (6). Additional, yet undefined signaling pathways may contribute to LAM cell persistence and lung involvement.

In exploring pleiotropic factors influencing LAM, we identified a common genetic variant in *NR3C1* (7), which encodes the glucocorticoid receptor (GR). We also observed nuclear localization of GR in LAM lung cells, together with a significant overlap between GR-dependent transcriptional programs and the LAM-specific gene expression signature, known as LAM^{core} (8). Previous biochemical studies have likewise detected GR protein in LAM tissue (9). In an integrative analysis of cancer cell lines, we further noted that the transcriptomic profile of LAM cells is relatively similar to that of pleural mesothelioma (10). Intriguingly, GR has been shown to promote a dormancy-like state in lung and pleural mesothelial cells by inducing expression of the cyclin-dependent kinase inhibitor CDKN1C (11). Given the established roles of GR in lung maturation and mesenchymal lineage commitment (12), these findings prompted us to investigate GR signaling in LAM using integrated cellular, molecular, and patient-based approaches.

Methods

Human samples and data

Retrospective LAM cohort. Data and blood samples of Spanish patients with LAM were compiled with the coordination of the Spanish LAM Association (AELAM) (13). Diagnoses were established at participating referral centers in accordance with guidelines (2). Blood samples were collected during two patient meetings at the same time of day (14:00 - 15:00 h) and the same time of year (late spring). Pulmonary function tests were not performed on the day of sample collection. Plasma samples were subjected to a maximum of three freeze–thaw cycles. Healthy premenopausal donors with an age distribution comparable to that of patients with LAM were recruited, and blood samples were obtained in late spring between 14:00 and 15:00. Participants provided written informed consent, and the study was approved by the ethics committee of the IDIBELL (LAM IMPROVE project PR104/20).

Prospective LAM cohort. Demographic, clinical, and laboratory data, together with plasma samples, were prospectively collected within the Polish LAM cohort under the IMPROVE project. The study was approved by the NTLDRI Bioethics Committee, and all participants provided written informed consent. Fasting venous blood samples were obtained between 08:00 and 09:30 h. Pulmonary function tests were conducted according to established guidelines (2). Chest imaging was performed using a 64-slice Revolution GSI CT scanner (GE Medical Systems). High-resolution CT (HRCT) scans were acquired with 1.25 mm collimation in the craniocaudal direction over a total scan time of approximately 3.5–4 seconds. For analysis, the lungs were divided into three anatomical zones: upper (apices to tracheal bifurcation), middle (tracheal bifurcation to inferior pulmonary vein), and lower (inferior vein to diaphragm). Cystic involvement in each zone was estimated as a percentage of lung volume replaced by cysts and categorized as follows: stage I (<25%, minimal), stage II (25–50%, mild), stage III (50–75%, moderate), and stage IV (>75%, severe or with architectural distortion or confluent cysts). The

staging system was adapted from Avila et al. (14). A global cystic involvement score was calculated by averaging the zonal grades. Cyst distribution was generally symmetrical between lungs.

Additional methodological details are provided in the supplementary material. The primer sequences are listed in **supplementary table S1**.

Results

GR transcriptional activity and clonogenic dependence in LAM/AML cell models

To assess GR signaling in a *TSC2*-mutant cell line, we treated *Tsc2*–/– MEFs with hydrocortisone (cortisol). Under basal conditions (medium supplemented with 5% CS-FBS), *Nr3c1* expression was substantially greater than *Nr3c2* (mineralocorticoid receptor; **supplementary table S2**). Following hydrocortisone treatment (2.75 μM for 8 hours), GR translocated to the nucleus (**Fig. 1A**). In addition, hydrocortisone upregulated canonical GR targets (*Gilz*, *Tgfb2*; two-tailed unpaired Student's *t*-test $P < 0.001$) without altering *Nr3c1* expression (**Fig. 1B**).

We next investigated the role of GR signaling in *Tsc2*–/– MEF clonogenicity using the selective GR modulator CORT125134 (relacorilant) (15). Treatment with CORT125134 at 10 nM, 300 nM, or 1 μM in 5% CS-FBS reduced colony-forming capacity (CFC) of *Tsc2*–/– MEFs (one-way ANOVA followed by pairwise comparisons with Holm-Sidak correction for multiple testing, $P = 7 \times 10^{-4}$; **Fig. 1C**). In contrast, hydrocortisone exposure (2.75 μM) increased CFC, an effect that was abolished by co-treatment with CORT125134 (one-way ANOVA with Holm-Sidak-adjusted post-hoc, $P = 1 \times 10^{-4}$; **Fig. 1D**). Of note, the hydrocortisone-mediated increase in clonogenicity was not observed in *Tsc2*+/+ MEFs (**Fig. 1E**).

NR3C1 was found to be significantly overexpressed in AML cells compared with normal stromal cells (dataset (16); Wilcoxon rank-sum test $P = 2.5 \times 10^{-4}$; **Fig. 2A**). We next evaluated GR dependency in *TSC2*–/– 621-101 AML cells (17), which also showed higher *NR3C1* expression relative to *NR3C2* (**supplementary table S3**). Hydrocortisone (2.75 μM, 5% CS-FBS; 8 hours) promoted GR nuclear localization and induced *GILZ* expression in these cells (**Fig. 2B**; **Fig. 2C**, two-tailed unpaired Student's *t*-test $P < 0.001$). Parallel to the findings in *Tsc2*–/– MEFs, hydrocortisone significantly increased CFC in *TSC2*–/– 621-101 cells, and this effect was abrogated by co-treatment with CORT125134 (one-way ANOVA with Holm-Sidak-adjusted post-hoc, $P = 5 \times 10^{-9}$; **Fig. 2D**). The control counterpart *TSC2*+/+ 621-103 cells do not form

discrete colonies under these conditions, and hydrocortisone did not increase any colony-like or proliferative pattern (**Fig. 2E**).

GR promotes *CDKN1C* expression in LAM/AML cells

Analysis of *CDKN1C* expression in human LAM and AML single-cell RNA-seq datasets (8, 16) showed significant overexpression in both contexts (Wilcoxon rank-sum test: $P = 5 \times 10^{-17}$ and $P = 2.6 \times 10^{-4}$, respectively; **Fig. 3A**). Consistently, LAM lung tissue samples ($n = 7$) showed nuclear CDKN1C staining in diseased cells (**Fig. 3B**). In addition, co-staining for CDKN1C and phospho-Ser235/236 ribosomal protein S6 (pS6), a marker of mTORC1 activity, showed co-localization within diseased cells (**Fig. 3C**).

Cdkn1c/CDKN1C expression was found to be significantly upregulated in both *Tsc2–/–* MEFs and *TSC2–/–* 621-101 cells following an 8-hour exposure to hydrocortisone (2.75 μM in 5% CS-FBS) (two-tailed unpaired Student's *t*-test *P* values < 0.01; **Fig. 3D**). To test whether *CDKN1C* induction is directly mediated by GR, we performed chromatin immunoprecipitation (ChIP) assays targeting three *CDKN1C* enhancers (18). Among these, enhancer #1 (chr11:2,800,200–2,800,300; hg19) showed significant GR enrichment in *TSC2–/–* 621-101 cells (two-tailed unpaired Student's *t*-test $P = 0.024$; **Fig. 3E**). Although *CDKN1C* is paternally imprinted, bulk LAM lung tissue showed no imprinting changes (**supplementary figure S1**), though low LAM cell abundance may mask subtle effects. Further supporting direct regulation of *CDKN1C* by GR, *Tsc2–/–* MEFs showed increased nuclear CDKN1C localization following hydrocortisone exposure, which was attenuated by co-treatment with CORT125134 (300 nM) (one-way ANOVA with Holm-Sidak-adjusted post-hoc, $P = 5 \times 10^{-8}$; **Fig. 3F**).

To determine whether GR broadly targets the transcriptional program that defines LAM, we queried the ChIP-Atlas, which aggregates >35,000 public ChIP-seq datasets uniformly processed (19). Intersecting the promoter-centric GR peak lists (±5 kb from transcription start site, score

≥50) with the LAM^{core} signature, showed the strongest GR-binding enrichment in mesenchymal stem cells (Fisher's exact test FDR-adjusted $P < 0.05$; **supplementary figure S2**).

GR-mediated regulation of AML cell cycle progression

Analysis of *Cdkn1c* expression at embryonic days 16.5 and 18.5 in a mesenchyme-specific *Nr3c1* deletion model (dataset (20) showed significant downregulation (two-way ANOVA, main effect of genotype $P = 7.8 \times 10^{-4}$; **Fig. 4A**). Next, building on the observed associations between *NR3C1*/GR and *CDKN1C* in human LAM and AML cells (**Fig. 3**), we assessed their combined impact on the cell cycle in *TSC2*–/– 621-101 cells. Hydrocortisone (2.75 μM) increased the G0/G1 fraction by 13%, and this rise reached 24% upon GR overexpression (**Fig. 4B**). Accordingly, combined hydrocortisone treatment and GR overexpression produced an additive increase in CDKN1C expression (14.4-fold vs. control; **Fig. 4C**), accompanied by robust upregulation of *GILZ* (two-tailed unpaired Student's *t*-test $P < 0.0001$; **Fig. 4D**). Dexamethasone, a potent and selective GR ligand, similarly enhanced *CDKN1C* expression in 621-101 cells (1 μM; 5% CS-FBS; 8 hours; **supplementary figure S3A**).

Because hydrocortisone produced an increase in a sub-G0 fraction, we evaluated whether this reflected apoptosis. Annexin staining indicated that neither hydrocortisone nor dexamethasone triggered apoptosis in *TSC2*–/– 621-101 cells or *Tsc2*–/– MEFs (**supplementary figure S3B**). Then, we quantified DAPI-based nuclear morpho-texture features under the same treatment conditions. Both glucocorticoids induced consistent reductions in nuclear solidity, mean DAPI intensity, and intensity dispersion (**supplementary figure S3C**), features compatible with chromatin reorganization and adoption of a slow-cycling state. Finally, and aligned with the well-established effect of rapamycin in inducing cell-cycle arrest (21–23), treatment of *TSC2*–/– 621-101 and *Tsc2*–/– MEFs with this compound (20 nM; 48 hours; 10% FBS) led to significant upregulation of *CDKN1C/Cdkn1c* and *NR3C1/Nr3c1* (two-tailed unpaired Student's *t*-test, $P \leq 0.01$; **Fig. 4E**).

Single-cell transcriptomic effects of GR Activation in AML Cells

To further characterize the molecular impact of GR signaling in *TSC2*–/– 621-101 cells, we performed scRNA-seq following exposure to either hydrocortisone (2.75 μM, 72 hours, 5% CS-FBS) or DMSO. As anticipated, *CDKN1C* was significantly upregulated by hydrocortisone (log fold-change = 0.25; $P = 0.002$). The gene signatures associated with GR-mediated transcriptional programs in breast cancer and fibroblasts (24, 25) were also robustly induced by hydrocortisone (**Fig. 5A**). Evaluation of G0/G1 cell cycle phase-specific gene signatures, including the Reactome G0 and Early G1 and Biocarta G1 Pathway, showed significant upregulation upon hydrocortisone treatment (**Fig. 5A**). Moreover, hydrocortisone-induced genes showed significant overlap with the LAM^{core} signature, with the shared genes primarily involved in developmental and differentiation processes (**Fig. 5B**).

Analysis of the scRNA-seq data identified a prominent population, cluster #1, which increased approximately 60-fold in response to hydrocortisone (**Fig. 5C**). Differential marker analysis of this cluster revealed expression of *EBF1* (a LAM^{core} gene), *PIK3R1* (significantly overexpressed in LAM cells; LAM Cell Atlas data (26), $P = 1 \times 10^{-12}$), and *NEAT1*, which, while not differentially expressed, was detected in 65% of LAM^{core} cells (LAM Cell Atlas data (26)) (**Fig. 5D**). Consistent with these findings, the LAM^{core} signature was significantly enriched in cluster #1 (Mann–Whitney U test, $P = 5 \times 10^{-84}$; **Fig. 5E**).

To further assess the link between GR signaling and LAM biology, we examined *Cdkn1c* and *Nr3c1* expression in a mouse model of LAM-like disease caused by conditional *Tsc2* deletion in the lung mesenchyme (27). Analysis of bulk RNA-seq data from sorted lung cell populations in this model indicated overexpression of *Cdkn1c* in the epithelial and mesenchymal compartments, and of *Nr3c1* in the mesenchymal compartment (two-tailed unpaired Student's *t*-test $P = 0.002$, 0.005, and 0.021, respectively; **Fig. 5F**).

Altered Plasma Cortisol–ACTH Axis in LAM and Its Association with Disease Stage

We next measured plasma cortisol, adrenocorticotropic hormone (ACTH), and the cortisol precursor 17α-hydroxyprogesterone (17-OH) in a retrospective cohort of patients with LAM (n = 37) and healthy female controls (n = 18) (13). All samples were collected during the afternoon under standardized conditions, and control samples were obtained in two independent batches (n = 9 and 9) to ensure reproducibility. Patients with LAM exhibited significantly elevated plasma ACTH and cortisol levels compared to controls (Wilcoxon rank-sum test P values = 0.012 and 0.0095, respectively; **Fig. 6A**). In turn, 17-OH levels were significantly reduced in the LAM group (Wilcoxon rank-sum test P = 0.008; **Fig. 6B**). There were no significant differences in hormone levels when patients with LAM were stratified by VEGF-D plasma concentration or rapamycin treatment (**supplementary fig. S4**).

The value distributions of ACTH and cortisol in the control group matched expected afternoon physiology (cortisol median 208 nmol/L; ACTH 2.7 pmol/L). Inspection of the distributions identified one high cortisol value in each group (356 nmol/L in controls; 692 nmol/L in LAM) and three high ACTH values in the LAM cohort (8.95, 8.52, and 10.1 pmol/L). Group differences for both hormones remained significant after excluding these values. Effect-size estimates indicated higher hormone levels in LAM: for cortisol, Cliff's delta was 0.44 (95% CI 0.17–0.69); for ACTH, 0.42 (95% CI 0.13–0.68). The Hodges–Lehmann median difference was 82 nmol/L for cortisol (95% CI 18–137) and 0.87 pmol/L for ACTH (95% CI 0.17–1.39).

We next evaluated plasma ACTH, cortisol and 17-OH progesterone in an independent prospective LAM cohort. Hormone concentrations did not differ between patients with S-LAM and TSC-LAM, or when stratified by VEGF-D levels, menopausal status, or rapamycin treatment (all $P > 0.2$). ACTH levels increased with radiological disease stage and were significant in both univariate (P = 0.023) and multivariate linear regression models adjusting for age, menopausal status, rapamycin use and LAM subtype (P = 0.025; **Fig. 6C**). Cortisol showed a similar stage-related pattern (**Fig. 6D**), although the association was not significant in the multivariate model.

POMC expression in LAM and AML cells

Given that ACTH derives from proteolytic processing of proopiomelanocortin (POMC) (28), we next measured circulating POMC in 5 controls and 15 LAM patients. All values were within the normal range (10-40 pmol/L), except for one LAM patient who exhibited an elevated concentration (300 pmol/L), potentially suggestive of Cushing's syndrome (**supplementary table S4**). Then, we detected POMC expression in diseased cells in all LAM lung samples examined (n = 7; **Fig. 7A**). However, we cannot exclude the possibility that the antibody may be detecting N-terminal POMC-derived peptides (N-POMC). We also analyzed single-cell transcriptomic data from the LAM Cell Atlas (26), which showed *POMC* transcripts in about 5% of LAM cells. The average expression level was not significantly different from that in other lung cell types. In contrast, analysis of scRNA-seq data from AMLs (16) revealed significant overexpression of *POMC* (Wilcoxon rank-sum test $P = 9 \times 10^{-123}$; **Fig. 7B**). The plasma ACTH levels in the prospective LAM cohort did not differ significantly between patients with and without AML and/or perivascular epithelioid cell tumors (P values > 0.3).

Discussion

Our findings suggest that LAM/AML cells are responsive to GR signaling, potentially contributing to their tumorigenic potential and disease progression. We propose a feed-forward axis in which diseased cells express POMC, leading to modest increases in ACTH and cortisol that, in turn, amplify GR activity and enhance target-gene expression such as CDKN1C. Supporting this model, an *NR3C1* eQTL was associated with increased LAM risk, the LAM^{core} signature overlaps GR-regulated transcriptional programs, and we detected GR and CDKN1C expression in LAM lung cells. Although several normal lung cell types (i.e., *TSC2* wild-type) also express GR/*NR3C1* (12, 29), GR-dependent clonogenicity in LAM/AML models, together with modest hormone elevations in patients, could point to therapeutic opportunities. Agents that inhibit adrenal steroidogenesis or antagonize GR (e.g., relacorilant) may suppress slow-proliferating cell states and merit evaluation in combination with drugs targeting proliferative diseased cells, noting that glucocorticoids themselves have not shown clinical benefit (2, 30, 31). Importantly, GR-induced CDKN1C expression would not trigger full growth arrest but instead support a slow-cycling state that may enhance cell survival under stress.

Slow-cycling or quiescence-like cell states are known to confer a survival advantage under metabolic or oncogenic stress (32). In LAM cells, biallelic loss of *TSC1* or *TSC2* drives chronic mTORC1 hyperactivation, likely creating sustained metabolic stress (33). GR signaling could then promote survival by simultaneously slowing G1-S progression via CDKN1C and modulating mTORC1 activity, as shown in other settings (34). Notably, dexamethasone-treated *TSC2*–/– 621-101 cells showed robust induction of *FKBP5*, which ranked among the top 10 upregulated transcripts in the scRNA-seq dataset. Given that *FKBP5* modulates mTORC1 signaling (35) and is found to be significantly overexpressed in LAM cells (data from the LAM Cell Atlas (26)), its induction may further influence diseased cell survival. It is also plausible that this slow-cycling survival state is dynamic and can revert to a more proliferative mode in response to specific metabolic cues or cellular conditions, potentially contributing to diseased-cell heterogeneity.

Future work dissecting the interplay between cell-cycle regulation and metabolic control in *TSC1/TSC2*-mutant cells could clarify the adaptive programs that support LAM cell survival.

GR signaling may also provide insights into the potential cell of origin in LAM. During lung development, GR regulates progenitor proliferation, airway architecture, and mesenchymal differentiation; loss of GR leads to hypercellularity and impaired maturation, while prolonged glucocorticoid exposure induces emphysematous changes (12, 36–38). These developmental roles suggest that heightened GR activity could permit survival of mesenchymal progenitors with *TSC1* or *TSC2* loss. GR also intersects with *NR2F2*, the top susceptibility locus in LAM (39), converging on pathways of metabolism, lineage specification, and matrix remodeling (40). Future *in vivo* models combining *Nr2f2*, *Nr3c1*, and *Tsc2* alterations may clarify early pathogenesis.

Our study has several limitations. Mechanistic assays were restricted to two *Tsc2/TSC2*-null cell models and to acute steroid exposures, which may not fully capture the chronic and heterogeneous LAM tissue environment. Chronic glucocorticoid exposure may also influence the microenvironment, and therefore sensitivity to GR signaling may vary across disease stages. Importantly, primary LAM cells cannot be cultured with currently available protocols, limiting the extent to which *in vitro* findings can be extrapolated to patient lesions. The retrospective patient cohort was relatively small, limiting statistical power and generalizability; findings, including the association with radiologic stage, require validation in larger cohorts. The retrospective and prospective cohorts were sampled at different times of day, and the early-morning hormonal surge is an established indicator of HPA-axis integrity. As a result, absolute hormone concentrations cannot be directly compared between the two cohorts, and cross-cohort differences should be interpreted with caution. Finally, despite integrating transcriptional, biochemical, and clinical data, contributions from additional pathways or systemic factors cannot be excluded.

Acknowledgments

This work is dedicated to the memory of Mari Guerrero, President of AELAM, whose pivotal role in advancing LAM research and tireless dedication to patient care remain an enduring legacy for all of us. We thank Miguel Angel Pardo, Frank Hause, and Javier A. Menendez for useful discussions.

Funding

This work was supported by the Spanish Association of LAM (AELAM); Fundació La Marató TV3 through Rare Diseases grant 202029-30; the Instituto de Salud Carlos III (co-funded by the European Regional Development Fund [ERDF], 'A way to build Europe') through grants PI21/0136 and PI24/01327; the Government of Catalonia (AGAUR) through grants SGR 2021-00184, 2021-00523, and SGR 2021-01537 (SGR-GRIMtra); and the National Institute of Health grant GM128675 to M.K.H. R.E. was supported by contract from the Departament de Salut, Generalitat de Catalunya, PERIS-PFI SLT017-20-000076; A.S. was supported by Generalitat de Catalunya AGAUR fellowship 2022-FI-B01068; and X.F. was supported by contract from the Ministry of Science, Innovation and Universities, TED2021-130626B-I00. We acknowledge the support of the Centres de Recerca de Catalunya (CERCA) Program to IDIBELL, IDIBGI, and IGTP.

Conflict of interest

H.H. is an employee and shareholder of Corcept Therapeutics. All other authors declare that they have no conflicts of interest relevant to the herein reported study.

Data availability

The scRNA-seq data generated in this study have been deposited in the Gene Expression Omnibus reference GSE302428.

References

1. Krymskaya VP, McCormack FX. Lymphangioleiomyomatosis: A monogenic model of malignancy. *Annu Rev Med*. 2017;68:69–83.
2. Johnson SR, et al. European Respiratory Society guidelines for the diagnosis and management of lymphangioleiomyomatosis. *Eur Respir J*. 2010;35(1):14–26.
3. Carsillo T, Astrinidis A, Henske EP. Mutations in the tuberous sclerosis complex gene *TSC2* are a cause of sporadic pulmonary lymphangioleiomyomatosis. *Proc Natl Acad Sci U S A*. 2000;97(11):6085–6090.
4. Saxton RA, Sabatini DM. mTOR signaling in growth, metabolism, and disease. *Cell*. 2017;169(2):361–371.
5. Prizant H, Hammes SR. Minireview: Lymphangioleiomyomatosis (LAM): The "other" steroid-sensitive cancer. *Endocrinology*. 2016;157(9):3374–3383.
6. Taveira-DaSilva AM, Pacheco-Rodriguez G, Moss J. The natural history of lymphangioleiomyomatosis: Markers of severity, rate of progression and prognosis. *Lymphat Res Biol*. 2010;8(1):9–19.
7. Farré X, et al. Evidence for shared genetic risk factors between lymphangioleiomyomatosis and pulmonary function. *ERJ Open Res*. 2022;8(1):00375–02021.
8. Guo M, et al. Single cell transcriptomic analysis identifies a unique pulmonary lymphangioleiomyomatosis cell. *Am J Respir Crit Care Med*. 2020;202(10):1373–1387.
9. Brentani MM, et al. Steroid receptors in pulmonary lymphangiomyomatosis. *Chest*. 1984;85(1):96–99.
10. Espín R, et al. Heterogeneity and cancer-related features in lymphangioleiomyomatosis cells and tissue. *Mol Cancer Res*. 2021;19(11):1840–1853.
11. Prekovic S, et al. Glucocorticoid receptor triggers a reversible drug-tolerant dormancy state with acquired therapeutic vulnerabilities in lung cancer. *Nat Commun*. 2021;12(1):4360.
12. Bird AD, et al. Glucocorticoid regulation of lung development: Lessons learned from conditional GR knockout mice. *Mol Endocrinol*. 2015;29(2):158–171.
13. Herranz C, et al. Histamine signaling and metabolism identify potential biomarkers and therapies for lymphangioleiomyomatosis. *EMBO Mol Med*. 2021;13(9):e13929.
14. Avila NA, et al. Sporadic lymphangioleiomyomatosis and tuberous sclerosis complex with lymphangioleiomyomatosis: comparison of CT features. *Radiology*. 2007;242(1):277–285.
15. Olawaiye AB, et al. Relacorilant and nab-paclitaxel in patients with platinum-resistant ovarian cancer (ROSELLA): An open-label, randomised, controlled, phase 3 trial. *Lancet*. 2025;405(10496):2205–2216.
16. Tang Y, Kwiatkowski DJ, Henske EP. Midkine expression by stem-like tumor cells drives persistence to mTOR inhibition and an immune-suppressive microenvironment. *Nat Commun*. 2022;13(1):5018.
17. Yu J, et al. Estradiol and tamoxifen stimulate LAM-associated angiomyolipoma cell growth and activate both genomic and nongenomic signaling pathways. *Am J Physiol Lung Cell Mol Physiol*. 2004;286(4):L694-700.
18. Cerrato F, De Crescenzo A, Riccio A. Looking for *CDKN1C* enhancers. *Eur J Hum Genet*. 2014;22(4):442–443.
19. Zou Z, et al. ChIP-Atlas 2021 update: A data-mining suite for exploring epigenomic landscapes by fully integrating ChIP-seq, ATAC-seq and Bisulfite-seq data. *Nucleic Acids Res*. 2022;50(W1):W175-182.
20. Bridges JP, et al. Glucocorticoid regulates mesenchymal cell differentiation required for perinatal lung morphogenesis and function. *Am J Physiol Lung Cell Mol Physiol*. 2020;319(2):L239–L255.
21. Metcalfe SM, et al. Rapamycin and p53 act on different pathways to induce G1 arrest in mammalian cells. *Oncogene*. 1997;15(14):1635–1642.

22. Huang S, et al. p53/p21(CIP1) cooperate in enforcing rapamycin-induced G(1) arrest and determine the cellular response to rapamycin. *Cancer Res*. 2001;61(8):3373–3381.
23. Fingar DC, et al. mTOR controls cell cycle progression through its cell growth effectors S6K1 and 4E-BP1/eukaryotic translation initiation factor 4E. *Mol Cell Biol*. 2004;24(1):200–216.
24. West DC, et al. Discovery of a glucocorticoid receptor (GR) activity signature using selective GR antagonism in ER-negative breast cancer. *Clin Cancer Res* 2018;24(14):3433–3446.
25. Leung CS, et al. Chronic stress-driven glucocorticoid receptor activation programs key cell phenotypes and functional epigenomic patterns in human fibroblasts. *iScience*. 2022;25(9):104960.
26. Du Y, et al. Lymphangioleiomyomatosis (LAM) Cell Atlas. *Thorax*. 2023;78(1):85–87.
27. Obraztsova K, et al. mTORC1 activation in lung mesenchyme drives sex- and age-dependent pulmonary structure and function decline. *Nat Commun*. 2020;11(1):5640.
28. Gallo-Payet N. 60 years of POMC: Adrenal and extra-adrenal functions of ACTH. *J Mol Endocrinol*. 2016;56(4):T135-156.
29. Travaglini KJ, et al. A molecular cell atlas of the human lung from single-cell RNA sequencing. *Nature*. 2020;587(7835):619–625.
30. McCormack FX, et al. Official American Thoracic Society/Japanese Respiratory Society Clinical Practice guidelines: Lymphangioleiomyomatosis diagnosis and management. *Am J Respir Crit Care Med*. 2016;194(6):748–761.
31. Taylor JR, et al. Lymphangioleiomyomatosis. Clinical course in 32 patients. *N Engl J Med*. 1990;323(18):1254–1260.
32. Sosa MS, Bragado P, Aguirre-Ghiso JA. Mechanisms of disseminated cancer cell dormancy: an awakening field. *Nat Rev Cancer*. 2014;14(9):611–622.
33. Blagosklonny MV. Rapamycin, proliferation and geroconversion to senescence. *Cell Cycle*. 2018;17(24):2655–2665.
34. Shimizu N, et al. Crosstalk between glucocorticoid receptor and nutritional sensor mTOR in skeletal muscle. *Cell Metab*. 2011;13(2):170–182.
35. Hausch F, et al. FKBPs and the Akt/mTOR pathway. *Cell Cycle*. 2013;12(15):2366–2370.
36. Massaro D, et al. Postnatal development of alveoli. Regulation and evidence for a critical period in rats. *J Clin Invest*. 1985;76(4):1297–1305.
37. Bird AD, et al. Mesenchymal glucocorticoid receptor regulates the development of multiple cell layers of the mouse lung. *Am J Respir Cell Mol Biol*. 2014;50(2):419–428.
38. Li A, et al. Deletion of mesenchymal glucocorticoid receptor attenuates embryonic lung development and abdominal wall closure. *PLoS One*. 2013;8(5):e63578.
39. Kim W, et al. A genome-wide association study implicates *NR2F2* in lymphangioleiomyomatosis pathogenesis. *Eur Respir J*. 2019;53(6).
40. Ashraf UM, Sanchez ER, Kumarasamy S. COUP-TFII revisited: Its role in metabolic gene regulation. *Steroids*. 2019;141:63–69.

Figure legends

Figure 1. GR activity and clonogenic potential in *Tsc2–/–* MEFs.

(**A**) Representative immunofluorescence images showing GR localization in *Tsc2–/–* MEFs under basal condition (5% CS-FBS) or after treatment with hydrocortisone (2.75 μM, 5% CS-FBS, 8 hours; $n = 3$ independent assays). Scale bars = 100 μm.

(**B**) Relative expression of canonical GR target genes *Gilz* and *Tgfb2*, and the GR gene *Nr3c1*, in *Tsc2–/–* MEFs under basal condition or following hydrocortisone treatment, as above ($n = 3$ independent assays; 3-5 replicates per assay). Statistical comparisons were performed using a two-tailed unpaired Student's *t*-test: ***$P < 0.001$, ****$P < 0.0001$; n.s., not significant.

(**C**) CFC of *Tsc2–/–* MEFs exposed to increasing concentrations of the selective GR antagonist CORT125134 (10 nM, 300 nM, 1 μM versus DMSO; $n = 3$ independent assays; 6 replicates per assay). Horizontal bars indicate the mean. One-way ANOVA with Holm-Sidak-adjusted post-hoc; $P = 7 \times 10^{-4}$. CORT125134 at 10 nM, 300 nM, and 1 μM significantly reduced colony formation compared with DMSO ($P = 0.033$, 0.0005, and 008, respectively). Significant pairwise differences are indicated (*$P < 0.05$, **$P < 0.01$, ***$P < 0.001$). No significant differences were observed among inhibitor doses.

(**D**) CFC in *Tsc2–/–* MEFs treated with CORT125134 (10 nM or 300 nM), hydrocortisone (2.75 μM), or both in combination ($n = 3$ independent assays; 6 replicates per assay). Horizontal bars indicate the mean. One-way ANOVA with Holm-Sidak-adjusted post-hoc; $P = 1 \times 10^{-4}$. CORT125134 at 10 nM and 300 nM significantly reduced clonogenic growth compared with DMSO ($P = 0.017$ and 0.002, respectively), whereas hydrocortisone increased colony formation ($P = 0.045$). Co-treatment with hydrocortisone and CORT125134 showed no significant differences relative to DMSO. Significant pairwise differences are indicated (*$P < 0.05$, **$P < 0.01$). Representative colony images are shown in the right panels.

(**E**) CFC in *Tsc2*+/+ MEFs. CORT125134 and/or hydrocortisone significantly reduced colony formation (one-way ANOVA with Holm-Sidak-adjusted post-hoc; $P = 3 \times 10^{-4}$). Representative colony images are shown in the right panels.

Figure 2. *NR3C1* expression and GR-dependent clonogenicity in *TSC2–/–* AML cells.

(**A**) Analysis of scRNA-seq data shows overexpression of *NR3C1* in human AML cells compared to normal stromal cells. Left: UMAP plot showing cell populations classified as AML (red) or normal (blue). Middle: UMAP plot displaying *NR3C1* expression levels across cells (log-normalized scale). Right: Dot plot summarizing the proportion of *NR3C1*-expressing cells and average expression in AML versus normal populations.

(**B**) Representative immunofluorescence images showing GR localization in *TSC2–/–* 621-101 under basal condition (5% CS-FBS) or after treatment with hydrocortisone (2.75 μM, 5% CS-FBS, 8 hours; $n = 2$ independent assays). Scale bars = 100 μm.

(**C**) Relative expression of *GILZ* in *TSC2–/–* 621–101 AML cells under basal conditions or after hydrocortisone exposure (2.75 μM, 5% CS-FBS; 8 hours) ($n = 3$ independent assays; 3 replicates per assay). Statistical comparison was made using a two-tailed unpaired Student's *t*-test: ****$P < 0.0001$.

(**D**) CFC of *TSC2–/–* 621–101 AML cells exposed to hydrocortisone (2.75 μM), CORT125134 (300 nM), or their combination ($n = 3$ independent assays; 6 replicates per assay). One-way ANOVA with Holm-Sidak-adjusted post-hoc; $P = 5 \times 10^{-9}$. CORT125134 at 300 nM reduced clonogenic growth compared with DMSO ($P = 0.018$), hydrocortisone increased colony formation ($P < 0.0001$), and co-treatment with hydrocortisone and CORT125134 significantly attenuated the hydrocortisone effect ($P < 0.0001$). Significant pairwise differences are indicated (*$P < 0.05$, ****$P < 0.0001$). Representative images of colony assays are shown in the right panels.

(**E**) CFC assay of *TSC2*+/+ 621–103 cells. This cell line does not form discrete colonies under these conditions and total staining intensity per area was quantified. Neither CORT125134 nor

hydrocortisone increased cell growth, although an increase was observed when both compounds were combined ($P < 0.0001$). Representative assay images are shown in the right panels.

Figure 3. GR promotes *CDKN1C* expression in LAM and AML cells.

(**A**) Left: Violin plot showing overexpression of *CDKN1C* in LAM cells compared to epithelial and stromal cell populations from human LAM lung scRNA-seq data. Asterisks indicate a significant difference among the three cell types by Kruskal–Wallis test (***$P < 2.2 \times 10^{-16}$). Middle: UMAP projection of human AML single-cell transcriptomes showing *CDKN1C* expression across normal and AML cells. Right: Dot plot summarizing the proportion of cells expressing *CDKN1C* and the average expression per group.

(**B**) Representative immunohistochemical staining for CDKN1C in lung tissue sections from patients with LAM. CDKN1C protein is predominantly localized to the nucleus in diseased cells. Scale bars = 50 μm. Placenta and pancreas tissues serve as positive controls.

(**C**) Representative image of dual immunofluorescence staining in LAM lung tissue showing co-localization of CDKN1C (magenta) and phosphorylated ribosomal protein S6 (pS6; green). DAPI marks nuclei (blue). The margin of the LAM lung nodule is delineated by a dashed white line. Scale bar = 50 μm.

(**D**) *Cdkn1c*/*CDKN1C* expression in *Tsc2–/–* MEFs and *TSC2–/–* 621–101 cells under basal conditions or after hydrocortisone treatment (2.75 μM, 5% CS-FBS; 8 hours) ($n = 2$ independent assays; 3 replicates per assay). Statistical comparisons were performed using a two-tailed unpaired Student's *t*-test: **$P < 0.01$, ***$P < 0.001$.

(**E**) ChIP assay for GR binding at three enhancer regions of *CDKN1C* in *TSC2–/–* 621–101 cells. GR binding was significantly enriched at enhancer #1 following hydrocortisone treatment ($n = 2$ independent assays; 3 replicates per assay). IgG was used as a negative control. Statistical comparisons were performed using a two-tailed unpaired Student's *t*-test: *$P < 0.05$, n.s., not significant.

(**F**) Left: Representative immunofluorescence images showing CDKN1C nuclear localization in *Tsc2–/–* MEFs exposed to vehicle, hydrocortisone (2.75 μM, 5% CS-FBS; 8 hours), CORT125134 (300 nM), or their combination. One-way ANOVA with Holm-Sidak-adjusted post-hoc test; $P = 5 \times 10^{-8}$. Hydrocortisone significantly increased nuclear CDKN1C compared with control ($P < 0.0001$), whereas CORT125134 alone did not differ from control. Co-treatment with hydrocortisone and CORT125134 significantly attenuated the hydrocortisone effect ($P < 0.001$). Significant pairwise differences are indicated (*$P < 0.05$, ***$P < 0.001$, ****$P < 0.0001$).

Figure 4. GR activation modulates cell cycle progression and CDKN1C expression in *TSC2*–/– AML cells.

(**A**) *Cdkn1c* expression is reduced in *Nr3c1*-mutant lungs during late embryonic development (embryonic days 16.5 and E18.5). Data correspond to the dataset GEO GSE30143. Horizontal bars indicate group means. Two-way ANOVA revealed significant main effects of genotype ($P = 7.8 \times 10^{-4}$) and developmental stage ($P = 9 \times 10^{-6}$), with no significant interaction ($P = 0.22$). *Cdkn1c* expression declined from E16.5 to E18.5 in controls ($P < 0.01$) and was further reduced in *Nr3c1–/–* embryos at E18.5 compared with controls ($P < 0.01$). Significant pairwise comparisons are indicated (**$P < 0.01$, ***$P < 0.001$).

(**B**) Flow cytometry analysis of DNA (propidium iodide stain) in *TSC2–/–* 621–101 cells following treatment with hydrocortisone (2.75 μM, 8 hours), GR overexpression, or their combination in 5% CS-FBS medium ($n = 2$ independent assays). An increase in G0/G1 cell subset is highlighted (purple). Hydrocortisone alone increased the G0/G1 fraction to 13%, while combined treatment with GR overexpression and hydrocortisone further increased this fraction to 24%.

(**C**) Immunoblot showing GR and CDKN1C protein levels in *TSC2–/–* 621–101 cells under the indicated conditions ($n = 2$ independent assays). TUBA serves as a loading control. Densitometric

analysis indicates additive induction of CDKN1C expression (14.4-fold) following GR overexpression and hydrocortisone treatment.

(**D**) *GILZ* expression in *TSC2–/–* 621–101 cells measured by quantitative assays under the indicated conditions (n =3 independent assays; 3 replicates per assay). GR overexpression enhanced hydrocortisone-induced *GILZ* expression. Statistical comparisons were performed using a two-tailed unpaired Student's t-test (****$P < 0.0001$).

(**E**) Rapamycin (20 nM, 48 hours, 10% FBS) increases *Cdkn1c/CDKN1C* and *Nr3c1/NR3C1* expression in *Tsc2–/–* MEF and *TSC2–/–* 621–101 cells ($n = 3$ independent assays; 3 replicates per assay). Statistical comparisons were performed using a two-tailed unpaired Student's t-test (*$P < 0.05$; **$P < 0.01$).

Figure 5. Single-cell transcriptional changes mediated by GR activation in *TSC2–/–* 621–101 cells.

(**A**) Gene set enrichment analysis of hydrocortisone- versus DMSO-treated *TSC2–/–* 621–101 cells. Signature scores were compared between conditions using the Wilcoxon rank-sum test, and significance is represented as $-\log_{10} P$ value.

(**B**) Venn diagram (left) showing significant overlap between genes upregulated by hydrocortisone and the LAM^{core} gene signature (Fisher's exact test $P = 7 \times 10^{-11}$). Gene ontology (GO) enrichment (right) of the overlapping gene set reveals functional categories primarily associated with developmental and differentiation processes.

(**C**) UMAP plots showing transcriptomic clustering of *TSC2–/–* 621–101 cells following treatment with DMSO (gray) or hydrocortisone (orange). Left: Cells grouped into nine distinct clusters based on single-cell transcriptomic profiles. Right: Proportion of cells in each cluster under DMSO or hydrocortisone conditions, highlighting a marked enrichment of cluster #1 following hydrocortisone treatment.

(**D**) Violin plots displaying normalized expression of *EBF1*, *PIK3R1*, and *NEAT1* across clusters. These genes are markers of cluster #1.

(**E**) Violin plot showing cluster-wise expression of the LAM^{core} signature.

(**F**) Log_2-normalized expression of *Nr3c1* (left) and *Cdkn1c* (right) in sorted lung populations from 8-week-old female $Tbx4^{LME\_Cre}Tsc2^{KO}$ (blue) and WT (black) mice: $CD45^+$, $EpCAM^+$, $CD31^+$, $PDPN^+$, and mesenchyme (all markers negative). Dots are individual mice (n = 3 per genotype); boxes show median and interquartile range. KO vs WT within each compartment was tested by two-tailed unpaired Student's t-test (*P < 0.05, **P < 0.01).

Figure 6. Altered plasma cortisol–ACTH axis in LAM and its association with disease stage.

(**A**) Plasma levels of ACTH (left) and cortisol (right) were significantly elevated in plasma from patients with LAM (n = 37) compared to healthy female controls (n = 18). Statistical comparisons were performed using a two-tailed Wilcoxon rank-sum test (*P < 0.05, **P < 0.01).

(**B**) Plasma levels of 17-OH were significantly reduced in plasma from patients with LAM compared to healthy female controls. Statistical comparison was performed using a two-tailed Wilcoxon rank-sum test (**P < 0.01).

(**C**) Linear regression analysis showing a positive association between plasma ACTH levels (log_2-transformed; as used in the modeling) and radiologic disease stage in a prospective LAM cohort. Each dot represents an individual patient; the red line denotes the regression fit, and the shaded area indicates the 95% CI.

(**D**) Violin plots showing plasma levels of ACTH, cortisol, and 17-OH stratified by radiologic disease stage.

Figure 7. POMC/*POMC* expression in LAM/AML diseased cells.

(**A**) Representative images of immunohistochemical staining of LAM lung tissues demonstrating POMC expression in diseased cells. Hypophysis serves as a positive control. Scale bars = 50 µm.

(**B**) UMAP projection of scRNA-seq data showing *POMC* expression in AML and normal stromal cells (left), with dot plot summarizing the percent of expressing cells and average expression (right).

Supplementary figure legends

Figure S1. Pyrosequencing methylation analysis of *KCNQ1OT1*:TSS-DMR in bulk LAM lung and control lung tissue. Graphs showing the level (peak) of methylation at each sequence position. The methylation percentages are indicated. The sample ID #12 and #16 were healthy, control lung tissue, and the rest were LAM lung tissue obtained from organ transplant surgeries.

Figure S2. Enrichment of GR binding in LAM^{core} genes across human cell types. Genome-wide GR ChIP-seq data were queried using the ChIP-Atlas platform to evaluate transcription factor binding enrichment at the LAM^{core} gene set. Significant enrichment (Fisher's exact test FDR-adjusted $P < 0.05$) was observed in several cell types, with the strongest signal in mesenchymal stem cells, followed by MCF10A (breast), adipocytes, HASM2 (lung), BEAS-2B (lung), HeLa (uterus), and A549 (lung). The y-axis shows fold enrichment relative to background.

Figure S3. Dexamethasone does not induce apoptosis in *TSC2–/–* 621-101 cells.

(**A**) *CDKN1C* expression in *TSC2–/–* 621–101 cells treated with dexamethasone (1 μM, 5% CS-FBS, 8 hours), demonstrating significant upregulation relative to basal condition ($n = 3$ independent assays; 3 replicates per assay). Statistical comparison was performed using a two-tailed unpaired Student's *t*-test: $^{**}P < 0.01$.

(**B**) Flow cytometric analysis of cell viability and apoptosis in *TSC2–/–* 621–101 (top panels) and *Tsc2–/–* MEFs (bottom panels) human cells treated for 24 hours with DMSO, hydrocortisone (25 μM), or dexamethasone (1 μM) ($n = 2$ independent assays). Right panels show the percentage of gated cells in each category (live cells, early apoptosis, late apoptosis, and late apoptosis/necrosis).

(**C**) Quantitative DAPI morpho-texture analysis of chromatin compaction. Representative DAPI-stained nuclei are shown color-coded for morphometric and intensity-texture features (solidity, mean intensity, and intensity dispersion/standard deviation). Right panels, violin plots summarize per-nucleus distributions across DMSO, dexamethasone, and hydrocortisone treatments.

Statistical significance was assessed using a Mann–Whitney test; ***$P < 0.001$. Scale bar = 10 μm.

Figure S4. Hormone profiling by VEGF-D status and rapamycin use. Plasma levels of ACTH (top) and 17-OH (bottom) were compared between healthy female controls (n = 18) and patients with LAM stratified by VEGF-D levels (high, $n = 13$; low, $n = 18$) or by rapamycin treatment status (on treatment, $n = 18$; off treatment, $n = 9$). One-way ANOVA with Holm-Sidak-adjusted post-hoc (*$P < 0.05$, **$P < 0.01$, ***$P < 0.001$; n.s., not significant).

Figure 1

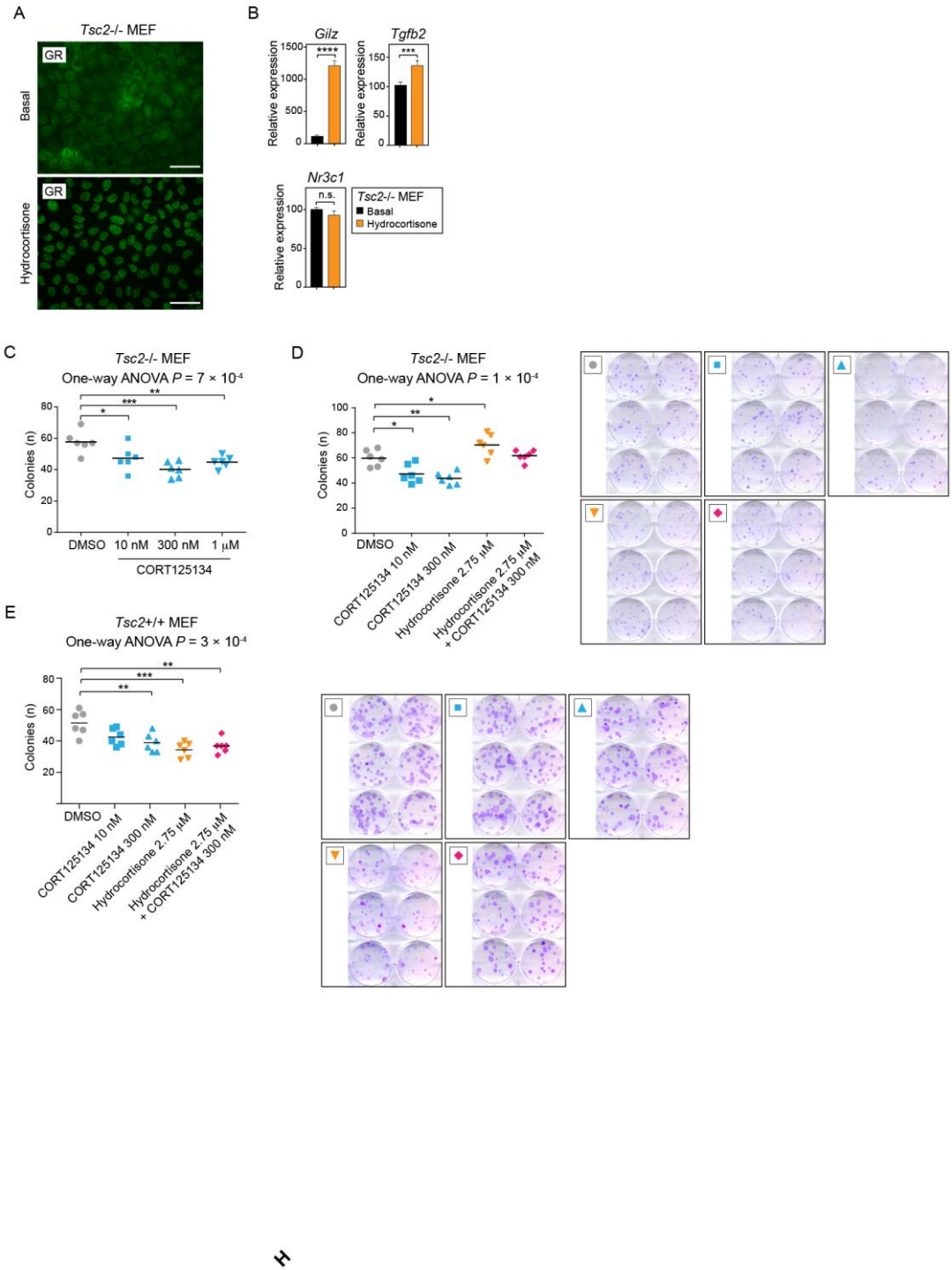

Figure 1

Figure 2

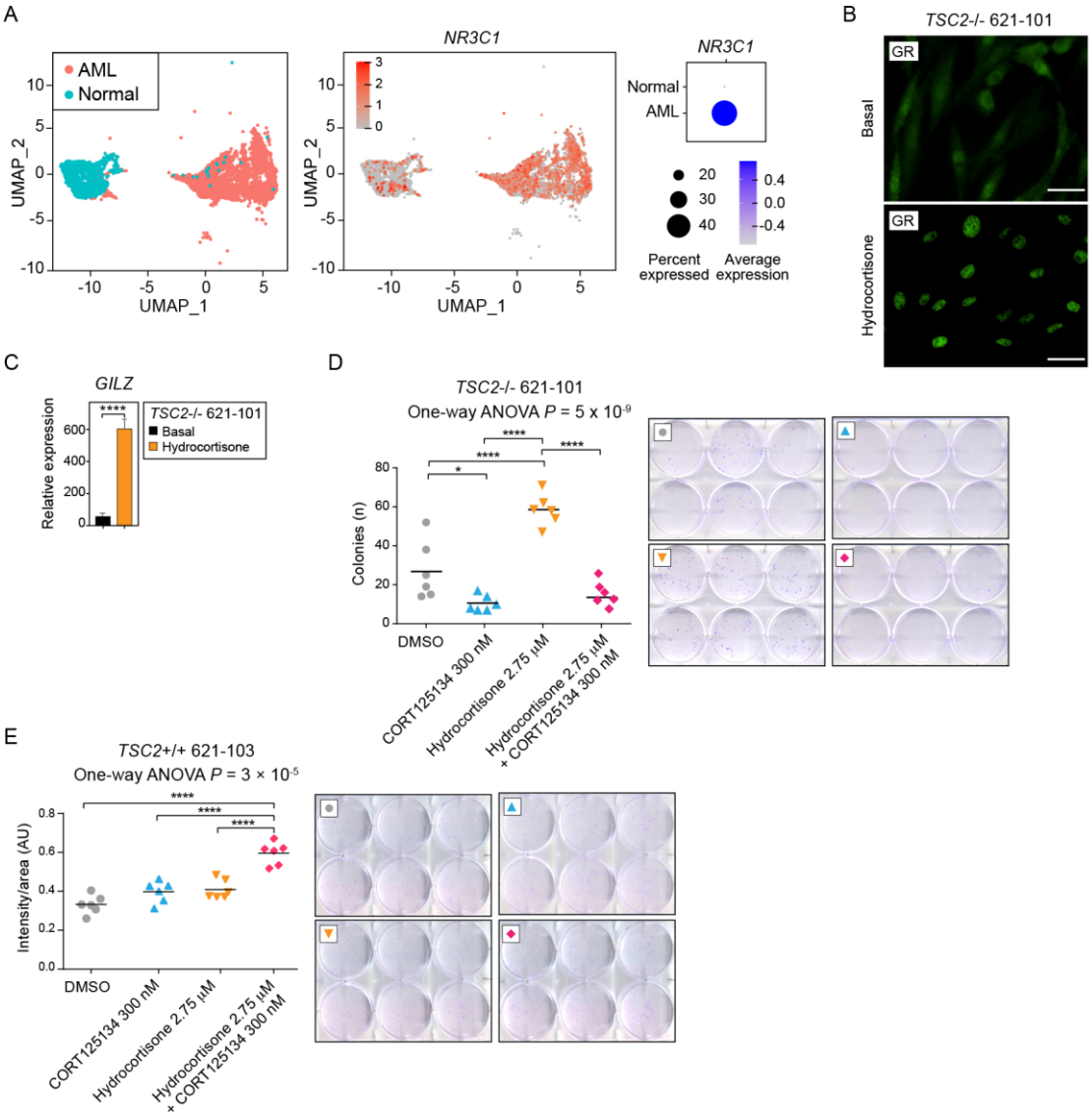

Figure 2

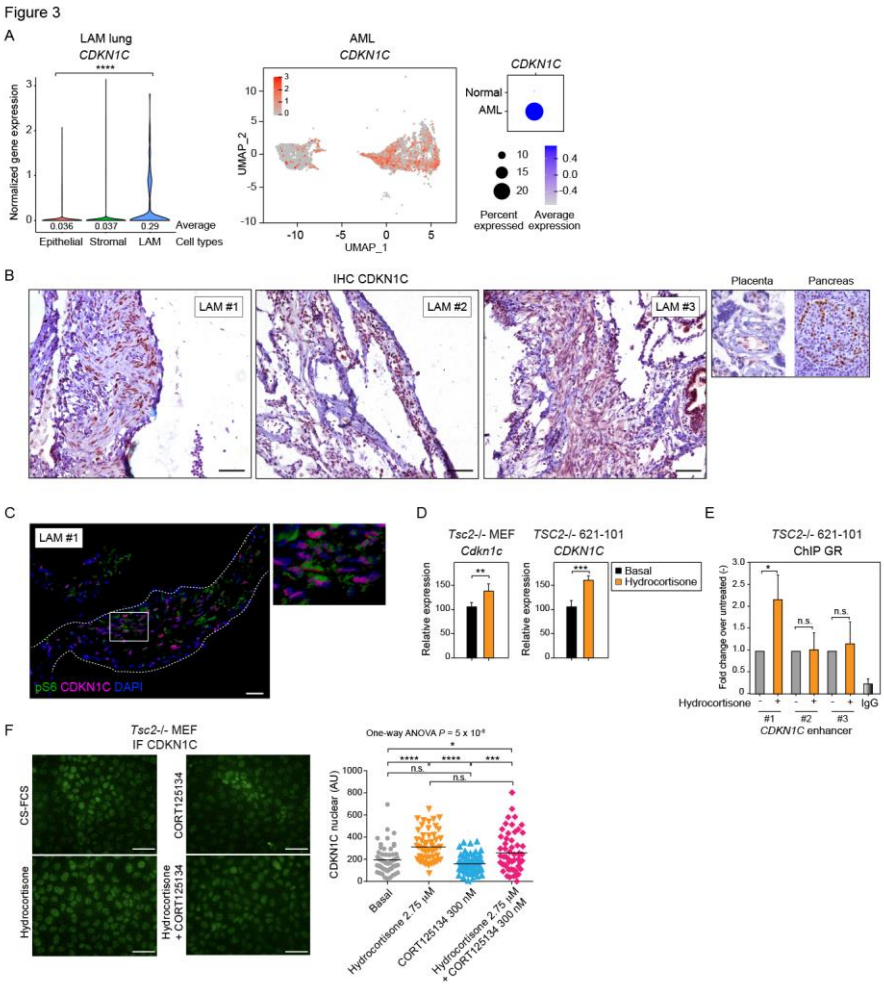

Figure 3

Figure 4

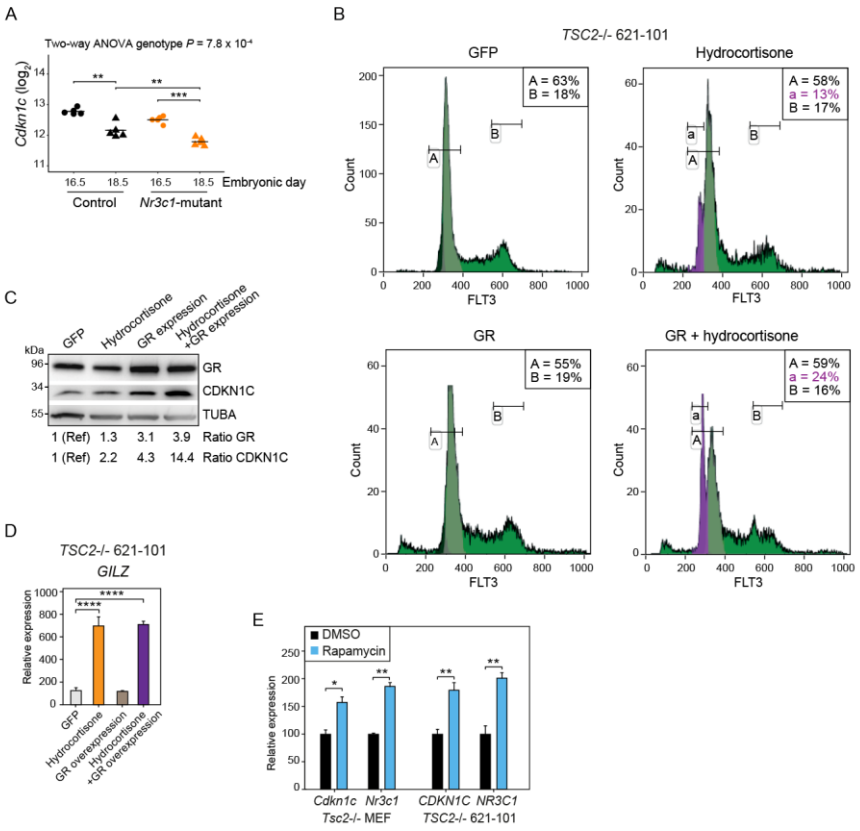

Figure 4

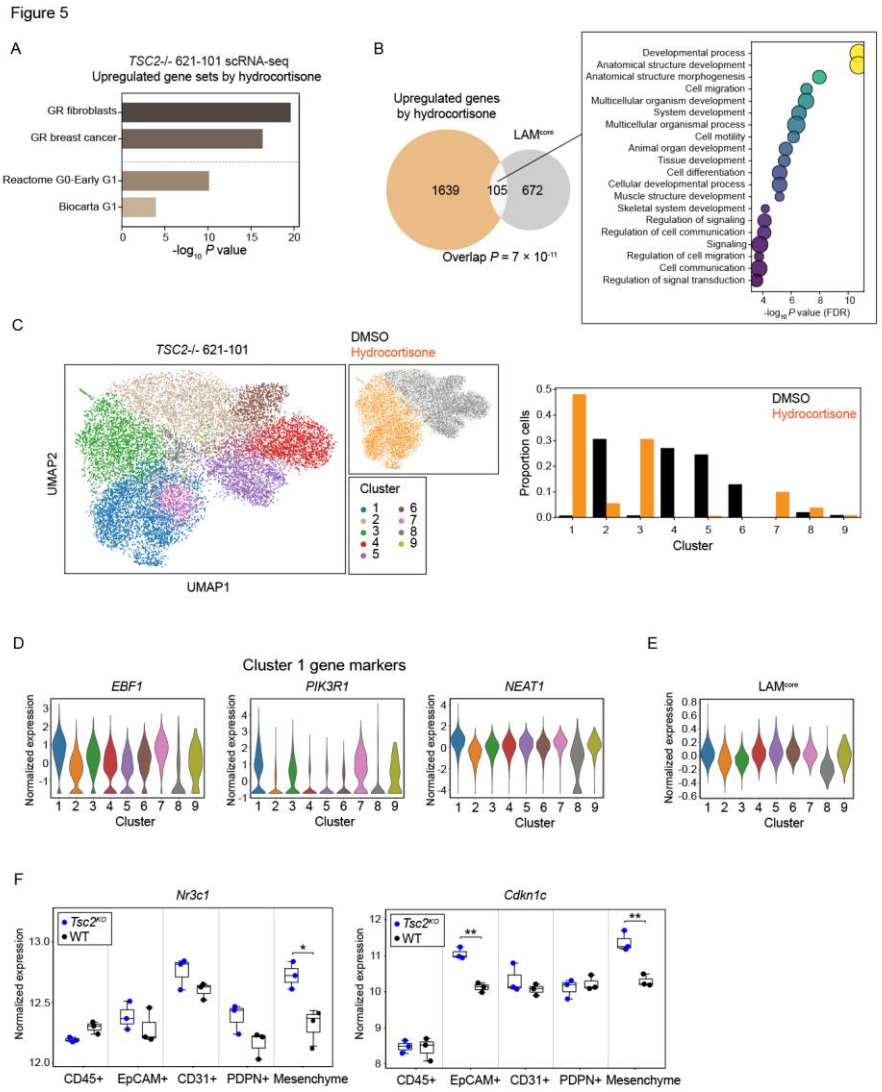

Figure 5

Figure 6

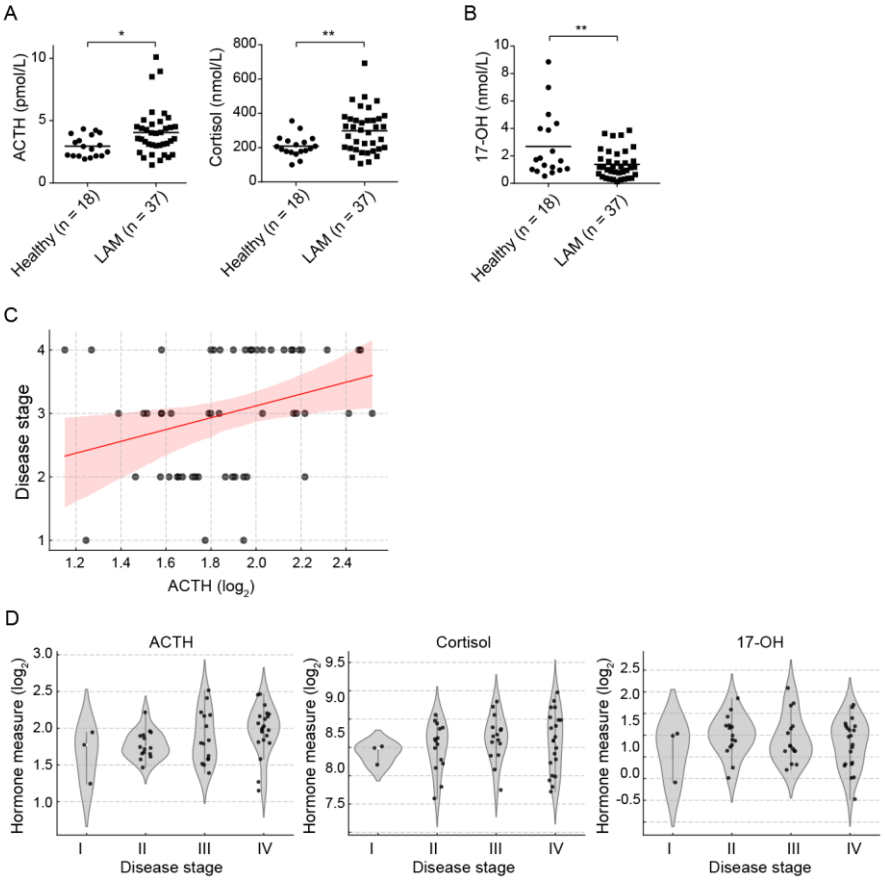

Figure 6

Figure 7

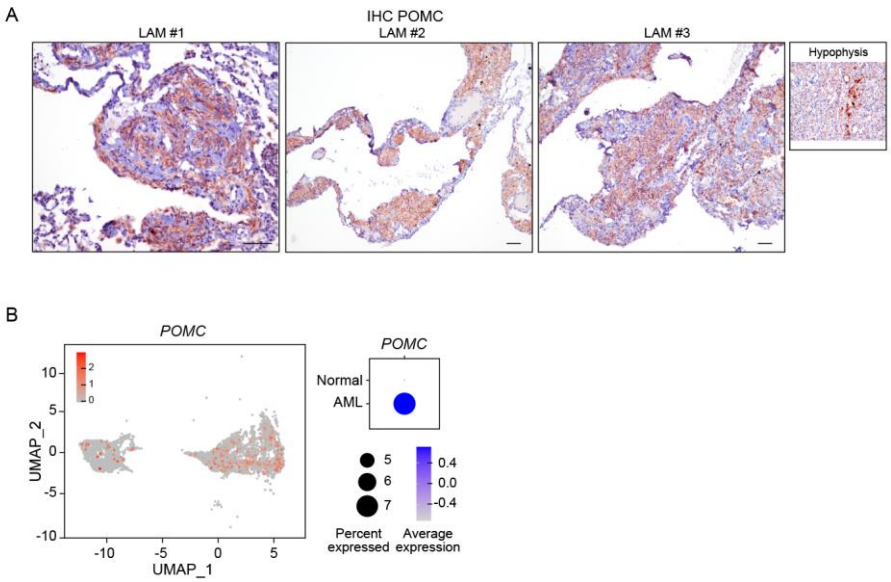

Figure 7

Exploring glucocorticoid receptor signaling in lymphangioleiomyomatosis

Supplementary methods

Cell culture

LAM cell models used in this study were *Tsc2*–/– mouse embryonic fibroblasts (MEFs) (1) and human *TSC2*–/– 621-101 angiomyolipoma (AML)–derived cells (2). Their control counterparts were *Tsc2*+/+ MEFs (1) and *TSC2*-reconstituted 621-103 cells (2). All cell lines were kindly provided by Prof. Elisabeth P. Henske (Center for LAM Research and Clinical Care, Brigham and Women's Hospital, Harvard Medical School, Boston, USA). Cell cultures were based on Dulbecco's Modified Eagle Medium (DMEM) supplemented with 10% fetal bovine serum (FBS; Gibco) or, when indicated, in serum-reduced medium, charcoal-stripped FBS (CS-FBS; Gibco). The colony-forming capacity (CFC) assays were performed by seeding 100-300 cells in 60-mm plates and growing for 7-14 days in the corresponding medium. Colonies were visualized by staining with crystal violet. The assays were performed in 3-6 replicates and at least three independent experiments.

LAM gene expression

Single-cell RNA sequencing (scRNA-seq) data from LAM lung tissue were analyzed according to the methods described in the original study (3), using the Gene Expression Omnibus (GEO) reference GSE135851. Only single cells with ≥500 expressed [unique molecular identifier (UMI) >0] genes and <10% UMIs mapping to mitochondrial genes were considered, except for the analysis of tissue sample LAM4, which included cells with ≥ 300 expressed (UMI >0) genes and <10% UMIs mapping to mitochondrial genes. Expression of each gene in a cell was determined by computing the natural logarithm of (10,000 UMIgene/UMIcell +1). Highly variable genes (n = 2,000) were used for dimension reduction, applying runPCA (PCA, n = 200) and the Uniform Manifold Approximation and Projection (UMAP) method (4). The previously defined LAM cell cluster was identified on the basis of the expression of specific genes, as previously described (3, 5). Gene signature scores were computed using the single-sample GSEA (ssGSEA) algorithm calculated in GSVA (version 1.43.1) (6). Normalized RNA-seq data from the lung mesenchymal *Tsc2* conditional knockout mouse model (GEO accession GSE139818) (7) were obtained and analyzed as processed matrices.

Reagents

Hydrocortisone and dexamethasone were purchased from Merck Life Science (catalogs H0888 and D4902, respectively), and rapamycin was purchased from Selleck Chemicals (catalog S1039). Relacorilant (developmental code name CORT125134) was obtained from Corcept Therapeutics. CORT125134) was used at 10 nM, 300 nM, and 1 μM, concentrations selected based on its high GR-binding affinity (inhibition constant Ki = 7–16 nM) and prior *in vitro* and *in vivo* pharmacologic studies (8, 9). The CellMiner NCI-60 screening dataset (10) indicates that relacorilant has weak intrinsic cytotoxicity, with half-maximal inhibitory concentration (IC_{50}) values typically falling within the low-micromolar range.

Western blot

Cell pellets were lysed in a 2% SDS 80mM Tris-HCl pH 6.8, sonicated, and protein concentration measured using the BCA Protein Assay (Thermo Fisher Scientific). Lysates were resolved in SDS-polyacrylamide electrophoresis gels and transferred to

polyvinylidene difluoride membranes (Sigma-Aldrich). Target proteins were detected using primary antibodies: anti-GR (dilution 1:1000; catalog 12041, Cell Signaling Technology), anti-CDKN1C (dilution 1:500; catalog HPA002924, Sigma-Aldrich), anti-TUBA (dilution 1:1000; catalog ab44928, Abcam), and anti-VINC (dilution 1:2000; catalog V9131, Sigma-Aldrich). Secondary antibodies were purchased from Santa Cruz Biotechnologies (1:2000 dilution; catalogs sc-2357 and sc-2005) and chemiluminescence detection performed with Novex™ ECL Chemiluminescent Substrate Reagent Kit (Thermo Fisher) in the ChemiDoc™ Imaging System (Bio-Rad). All Western blot assays were performed in at least two independent experiments.

Targeted gene expression

For gene expression quantification, total RNA was isolated from cells using TRIzol reagent (Thermo Fisher) and complementary DNA (cDNA) synthesized using the High-Capacity cDNA Reverse Transcription Kit (Thermo Fisher), following the manufacturer's protocol. Gene expression values were measured using reverse-transcription polymerase chain reactions with SYBR Green (Applied Biosystems). The mouse and human control genes were *Ppia* and *ACTB*, respectively, and expression level differences were computed by the ΔΔCt method (11). The qPCR assays were performed with 3-5 technical replicates in at least two independent experiments. The primer sequences are listed in **supplementary table S1**.

Immunohistochemistry

Formalin-fixed paraffin-embedded LAM lung tissue from seven patients was analyzed in this study by immunohistochemistry (IHC) assays. These were performed on paraffin sections using antigen retrieval with citrate pH 6.0 (anti-CDKN1C; dilution 1:50; catalog HPA002924, Sigma-Aldrich) or EDTA pH 9.0 (anti-POMC-derived peptide; dilution 1:2000; catalog HPA063644, Sigma-Aldrich) buffer. Endogenous peroxidase was blocked by pre-incubation in a solution of 3% H_2O_2, prepared in 1× phosphate-buffered saline with 10% goat serum. Slides were incubated overnight at 4°C with primary antibody diluted in blocking solution and detected with secondary antibody for 1 hour at room temperature using the DAKO EnVision™ System. Sections were counterstained with hematoxylin and examined under a Nikon Eclipse 80i microscope. The assays included defined positive tissue controls for each antibody-target.

Immunofluorescence

The cells were grown on coverslips, fixed with paraformaldehyde 4%, incubated overnight at 4°C with primary antibody diluted in blocking solution, and detected with secondary antibody for 1 hour at room temperature. The cells were counterstained with DAPI, mounted with coverslips in Fluoromount® Aqueous Mounting Medium (Sigma-Aldrich), and visualized using a DM6000 fluorescence microscope (Leica). The assays were performed in three independent experiments. The primary antibodies were anti-GR (dilution 1:1000; catalog 12041, Cell Signaling Technology), anti-CDKN1C (dilution 1:100; catalog HPA002924, Sigma-Aldrich), and anti-phospho-Ser235/236 ribosomal protein S6 (pS6; catalog 2211, Cell Signaling Technology).

Methylation pyrosequencing

Standard bisulfite PCR reactions were performed including the reverse primer biotinylated to amplify the *CDKN1C* region of interest (12, 13). Briefly, the biotinylated PCR products were mixed with binding buffer and streptavidin-coated polystyrene beads, incubated at 65 °C, DNA denaturated using 0.5 M NaOH, and single-stranded DNA

hybridized to sequencing primers dissolved in annealing buffer. For sequencing, a primer was designed to the opposite strand to the biotinylated primer used in the PCR reaction. The pyrosequencing reactions were carried out on a PyroMark Q96 instrument. The peak heights were determined using Pyro Q-CpG1.0.9 software (Biotage).

Chromatin immunoprecipitation

Crosslinking of proteins with DNA, fragmentation, and preparation of soluble chromatin followed by immunoprecipitation with specific antibodies were performed as previously described (14). Briefly, 5 x 10^6 of *TSC2*–/– 621-101 and *TSC2*-reconstituted 621-103 AML cells (2) treated or not with hydrocortisone were incubated with 1% (v/v) formaldehyde in pre-warmed phosphate buffered saline (PBS) for 10 min at 37°C. Cells were then washed in cold PBS, harvested and lysed to isolate nuclei in hypotonic buffer containing 5 mM PIPES at pH 8.0, 85 mM KCl and 0.5% NP-40. Nuclei were then resuspended, lysed in a buffer containing 1% SDS, 10 mM EDTA pH 8.0, and 50 mM Tris/HCl pH 8.1, and sonicated in 15 mL tubes with Bioruptor sonication device (7 times 30 s ON, 30 s OFF) to yield chromatin sizes of 150–300 bp. Thirty µg of DNA/sample were used for immunoprecipitation with 7.5 µg anti-GR (catalog D6H2L, Cell Signaling Technology) and with the same amount of anti-rabbit IgG (catalog 2729, Cell Signaling Technology). Immunoprecipitated and input DNAs were purified and subjected to qPCR analysis using the primers amplifying the GR-bound enhancers (#1-3) described in *CDKN1C* (12, 13). Quantification of chromatin immunoprecipitation was performed by real-time PCR using Roche LightCycler® 480 system. The fold enrichment of target sequence in immunoprecipitated (IP) compared to input (Ref) fractions was calculated using the comparative Ct (the number of cycles required to reach a threshold concentration) method with the equation $2^{Ct(IP)-Ct(Ref)}$. The assays were performed in two independent experiments. The primer sequences are listed in **supplementary table S1**.

GR overexpression and cell cycle

TSC2–/– 621-101 AML cells were grown in 5% charcoal-stripped FCS medium for 24 hours, transfected with pRSV-GR construct (15) or GFP-expression vector (pEGFP-C1) using Lipofectamine 2000 (Thermo Fisher Scientific) for 4 hours and then replaced with fresh 5% CS-FBS media. Forty-eight hours after transfection the cells were stained with propidium iodide for 10 min and the cell cycle profile analyzed using the Gallios cytometer (Beckman Coulter).

Nuclear features

DAPI-stained nuclei were imaged using identical acquisition settings across all treatment conditions (DMSO, dexamethasone, hydrocortisone). Nuclear segmentation and quantitative morphometric analysis were performed in ImageJ/Fiji (16). Briefly, images were pre-processed using background subtraction and adaptive thresholding, followed by morphological filtering and watershed separation to resolve touching nuclei. For each nucleus, solidity, mean DAPI intensity, and intensity dispersion (standard deviation of pixel intensities) were extracted using the Analyze Particles and Measure Texture functions. The measurements were exported as single-cell values and 100 cells were analyzed in each condition. Distributions were compared using the Mann–Whitney U test with Bonferroni correction.

Single-cell RNA sequencing

TSC2–/– 621-101 cells were cultured in DMEM/F-12 supplemented with 10% FBS, seeded 24 hours prior to steroid depletion, then switched to phenol red–free medium

containing 5% CS-FBS for 24 hours. Subsequently, cells were treated for 72 hours with either vehicle control or 2.75 μM hydrocortisone. Cell suspensions (>90% viability) were washed in PBS containing 0.04% bovine serum albumin (BSA), filtered through a 40-μm mesh, counted, and loaded onto a Chromium Controller (10x Genomics) using Single Cell 3′ v3.1 chemistry. Libraries were prepared according to the manufacturer's instructions and sequenced on an Illumina NovaSeq 6000 platform. Raw sequencing data were processed with Cell Ranger (v6.1.2; 10x Genomics) using the GRCh38-2020-A reference genome. Analyses were conducted in Python 3.11 using Scanpy (v1.10.1). Per-cell quality metrics were calculated, and cells were retained if they met all of the following criteria: ≥500 and ≤ 35,000 UMIs, ≥250 detected genes, and ≤ 15% mitochondrial transcripts. Genes detected in ≤3 cells were excluded. Counts were library-size normalized to 10,000 UMIs per cell and log-transformed. Highly variable genes (n = 3,295) were identified using seurat_v3, combining lists of variable genes determined separately in each treatment condition. The scaled expression matrix was subjected to principal component analysis (PCA), and the first 30 principal components (explaining 84% of variance) were used to construct a k-nearest neighbor graph (k = 15). Cells were embedded in two dimensions using UMAP and clustered using the Leiden algorithm (resolution = 0.5) (17). The association between cluster membership and treatment condition was evaluated using a χ^2 test, with false discovery rate (FDR) controlled by the Benjamini–Hochberg procedure (18). Differential gene expression between hydrocortisone and vehicle-treated cells was assessed both globally and within each cluster using t_test_overestim_var as implemented in *Scanpy*. Genes with absolute $\log_2$ fold-change ≥ 0.25 and FDR < 0.05 were considered significant. The previously defined LAM^{core} gene signature (3) was intersected with the expressed gene set (genes n = 99) and enrichment scores were computed for each cell using sc.tl.score_genes (z-scored). Enrichment distributions were compared across clusters using the Kruskal–Wallis test followed by pairwise Mann–Whitney U tests with FDR adjustment.

Quantification of circulating steroid hormones

The assays were performed at the ISO 15189-accredited Clinical Laboratory of the University Hospital of Bellvitge. Plasma concentration of cortisol was determined using the electrochemiluminescence immunoassay technique in the Cobas® 8000 Analyzer (Cortisol II reference 06687733-190; Roche Diagnostics; reference range 133–537 nmol/L). The chemiluminescent immunoassay technology in the LIAISON® Analyzer (DiaSorin) was used to determine ACTH (LIAISON® ACTH catalog 313221; reference range 2–12 pmol/L). A solid-phase competitive ELISA kit (EIA-1292; DRG Instruments GmbH) was used to measure 17α-hydroxyprogesterone: the reference values in our clinical center were 0.3–7.0 (men >18 years old: 1.5–6.4 nmol/L; women >18 years old, follicular phase: 0.3–2.4 nmol/L; women >18 years old, luteal phase: 1.8–7.0 nmol/L; women >18 years old, ovulation phase: 0.9–4.2 nmol/L; and women >18 years old, postmenopausal: 0.4–1.5 nmol/L), respectively. None of the measured hormones showed significant differences between the subgroups of healthy women included as controls in this study. POMC and pro-ACTH, the precursors of ACTH, were quantified in human plasma using a 2-site immunometric assay (19, 20). Briefly, monoclonal antibody A1A12 (research resource identifier: 2756529) which binds the central ACTH region 10-18, was coated on the ELISA plate. After the addition of samples or standards (POMC purified from a human small cell lung carcinoma cell line), a biotin-labelled N1C11 monoclonal antibody (specific for the gamma MSH region of POMC; research resource identification 2756530) was added with avidin linked horseradish peroxidase. This assay has a

sensitivity of 10 pmol/L, is specific for POMC and pro-ACTH, and does not detect ACTH (21). Reference ranges for ACTH-related disorders were defined (21).

Statistical analysis

All experiments shown are representative of at least three independent biological replicates, unless otherwise indicated. The analyses were performed using GraphPad Prism 9 (GraphPad Software) or R software (version 4.3.2). Parametric tests (two-tailed unpaired Student's *t*-test or one-way ANOVA with Holm-Sidak-adjusted post-hoc) were applied to *in vitro* experimental data, which were generated under controlled conditions and showed approximately normal distributions. For patient hormone and clinical data, where normality could not always be assumed, non-parametric tests (Wilcoxon rank-sum, Kruskal–Wallis with Dunn's post hoc) were used. Statistical significance was defined as $P < 0.05$ ($*P < 0.05$, $**P < 0.01$, $***P < 0.001$, and $****P < 0.0001$). Results presented in histograms are displayed as means with error bars indicating standard deviation (sd).

References

1. Zhang H, et al. Loss of Tsc1/Tsc2 activates mTOR and disrupts PI3K-Akt signaling through downregulation of PDGFR. *J Clin Invest*. 2003;112(8):1223–1233.
2. Yu J, et al. Estradiol and tamoxifen stimulate LAM-associated angiomyolipoma cell growth and activate both genomic and nongenomic signaling pathways. *Am J Physiol Lung Cell Mol Physiol*. 2004;286(4):L694-700.
3. Guo M, et al. Single cell transcriptomic analysis identifies a unique pulmonary lymphangioleiomyomatosis cell. *Am J Respir Crit Care Med*. 2020;202(10):1373–1387.
4. Becht E, et al. Estimating the population abundance of tissue-infiltrating immune and stromal cell populations using gene expression. *Genome Biol*. 2016;17(1):218.
5. Espín R, et al. Heterogeneity and cancer-related features in lymphangioleiomyomatosis cells and tissue. *Mol Cancer Res*. 2021;19(11):1840–1853.
6. Hänzelmann S, Castelo R, Guinney J. GSVA: Gene set variation analysis for microarray and RNA-seq data. *BMC Bioinformatics*. 2013;14:7.
7. Obraztsova K, et al. mTORC1 activation in lung mesenchyme drives sex- and age-dependent pulmonary structure and function decline. *Nat Commun*. 2020;11(1):5640.
8. Hunt HJ, et al. Identification of the clinical candidate (R)-(1-(4-fluorophenyl)-6-((1-methyl-1H-pyrazol-4-yl)sulfonyl)-4,4a,5,6,7,8-hexahydro-1H-pyrazolo[3,4-g]isoquinolin-4a-yl)(4-(trifluoromethyl)pyridin-2-yl)methanone (CORT125134): A selective glucocorticoid receptor (GR) antagonist. *J Med Chem*. 2017;60(8):3405–3421.
9. Greenstein AE, Hunt HJ. Glucocorticoid receptor antagonism promotes apoptosis in solid tumor cells. *Oncotarget*. 2021;12(13):1243–1255.
10. Reinhold WC, et al. CellMiner: A web-based suite of genomic and pharmacologic tools to explore transcript and drug patterns in the NCI-60 cell line set. *Cancer Res*. 2012;72(14):3499–3511.
11. Livak KJ, Schmittgen TD. Analysis of relative gene expression data using real-time quantitative PCR and the 2(-delta delta C(T)) Method. *Methods San Diego Calif*. 2001;25(4):402–408.
12. Cerrato F, De Crescenzo A, Riccio A. Looking for *CDKN1C* enhancers. *Eur J Hum Genet*. 2014;22(4):442–443.
13. Prekovic S, et al. Glucocorticoid receptor triggers a reversible drug-tolerant dormancy state with acquired therapeutic vulnerabilities in lung cancer. *Nat Commun*. 2021;12(1):4360.

14. Strutt H, Paro R. Mapping DNA target sites of chromatin proteins *in vivo* by formaldehyde crosslinking. *Methods Mol Biol*. 1999;119:455–467.
15. Hagen G, et al. Tissue-specific expression, hormonal regulation and 5'-flanking gene region of the rat Clara cell 10 kDa protein: Comparison to rabbit uteroglobin. *Nucleic Acids Res*. 1990;18(10):2939–2946.
16. Schindelin J, et al. Fiji: An open-source platform for biological-image analysis. *Nat Methods*. 2012;9(7):676–682.
17. Traag VA, Waltman L, van Eck NJ. From Louvain to Leiden: Guaranteeing well-connected communities. *Sci Rep*. 2019;9(1):5233.
18. Benjamini Y, Hochberg. Controlling the false discovery rate: A practical and powerful approach to multiple testing. *J Royal Stat Soc*. 1995;57(1):289–300.
19. Stovold R, et al. Neuroendocrine and epithelial phenotypes in small-cell lung cancer: implications for metastasis and survival in patients. *Br J Cancer*. 2013;108(8):1704–1711.
20. Crosby SR, et al. Direct measurement of the precursors of adrenocorticotropin in human plasma by two-site immunoradiometric assay. *J Clin Endocrinol Metab*. 1988;67(6):1272–1277.
21. Harno E, et al. POMC: The physiological power of hormone processing. *Physiol Rev*. 2018;98(4):2381–2430.